Multi-modal commutative dynamics in semi-crystalline polymers undergoing multiple shape memory behavior

Xiaodong Wang[1], Haibao Lu[1,5], Galina Gorbacheva[2,5], Mokarram Hossain[3] and Yong Qing Fu[4]

[1]National Key Laboratory of Science and Technology on Advanced Composites in Special Environments, Harbin Institute of Technology, Harbin 150080, P.R. China

[2]Mytishchi Branch of Federal State Budgetary Educational Institution of Higher Education, Bauman Moscow State Technical University, Mytishchi 141005, Russia

[3]Zienkiewicz Centre for Computational Engineering, College of Engineering, Swansea University, Swansea, UK

[4]Smart Materials and Surfaces Laboratory, Faculty of Engineering and Environment, Northumbria University, Newcastle upon Tyne NE1 8ST, UK

[5]E-mail: luhb@hit.edu.cn and gorbacheva@mgul.ac.ru

Abstract: Semi-crystalline polymers offer great opportunities for design and tuning of multi-shape memory effects (multi-SMEs) through their programmable melting transitions. However, coexistence of amorphous and crystalline components as well as their interfaces result in complex cooperative dynamics. In this study, we propose an extended three-phase model to describe the commutative and cooperative dynamics in semi-crystalline shape memory polymers (SMPs) undergoing multi-SMEs. A three-phase model and Takayanagi principle are firstly applied to study the cooperative dynamics of amorphous/crystalline components and their interfaces. Phase transition theory and modified Avrami theory are further applied to model the cooperative dynamics of glass and melting transitions, respectively. Commutative dynamics and glass/melting transitions have been investigated in order to realize custom-designed

multi-SMEs and shape recovery behaviors. Finally, effectiveness of the newly established model was demonstrated to predict triple-SMEs and quadruple-SMEs in semi-crystalline polymers reported in literature, and the theoretically obtained results show good agreements with the experimental ones.

Keywords: Semi-crystalline polymer; commutative dynamics; shape memory effect

1. Introduction

Shape memory polymer (SMP) is one of the most popular soft matters which have the capabilities of recovery of highly pre-deformed shapes in response to external stimuli, such as heat, solvent, light, electric or magnetic fields [1-6]. Different from the conventional shape-change soft matters, the SMP can have a temporarily fixed shape and then regain its permanent shape due to its special thermodynamics. Therefore, it has a great numbers of practical applications for biomedical devices, textiles, actuators and drug delivery systems [7-11].

Unlike the conventional “dual-stage SMPs” which has a single transition zone and can only fix one temporary shape, multi-SMPs are capable of fixing two or more temporary shapes in the sequentially programmed processes [10], and then regain their temporary multiple shapes upon step-by-step thermal or other stimulations. To achieve this, the multi-SMPs are necessary to have two or more shape-fixing mechanisms distinguished by their different thermal transitions [12]. Among various types of multi-SMPs, semi-crystalline polymers are the most common material systems [13-15], since they easily display two well-separated transitions, e.g., one from the glass transition of their amorphous component and the other from the melting transition of the crystalline component [16]. Moreover, quadruple-SMEs were also discovered in such material systems by incorporating poly(L-lactic acid) (PLLA)

and poly(D-lactic acid) (PDLA) into a polyurethane matrix, and such triblock polymers have two glass transitions and two melting transitions which are used to generate different temporary shapes [17].

However, majority of the previous studies have been focused on the amorphous SMPs, using the classic phase transition theory [18,19] and Maxwell models [20,21]. Due to the complex morphology of their internal structures, the relaxation behavior of semi-crystalline polymers is really hard to model. Not only the glass transition of amorphous component, but also the melting transition of crystalline component should be considered. According to the three-phase model [22], the semi-crystalline polymers have three components, e.g., the mobile amorphous component, rigid amorphous component and crystalline component. The rigid amorphous component is the amorphous segments which are within the spherulitic structures, and it has no contribution to the glass transition event [23]. Meanwhile, relaxation of the mobile amorphous component is resulted from the cooperative motions of their neighbors and interspaces [24]. Whereas the crystalline component significantly confines the cooperative relaxation motions, thus playing an essential role to influence the glass transition [25].

Establishing the constitutive models of the semi-crystalline polymers is crucial to reveal the working mechanisms of viscoelastic relaxation behavior. Ge et. al utilized multi-branch models to explain the finite deformation and recovery behavior of semi-crystalline polymers [26,27]. Moon et. al applied Abaqus finite element analysis to study triple-shape recovery behavior of a semi-crystalline stent [28]. However, the cooperative dynamics between crystalline and amorphous components has not been studied in most of these previous reports. Therefore, it is necessary to propose an

effective and theoretical approach to characterize the intrinsic molecular structure and thermodynamics of the multi-SMPs, in order to identify their working principle.

In this study, a multi-modal dynamic model is firstly developed to explain the unique relaxation characteristics of semi-crystalline SMPs. Based on the three-phase model [22] and the Adam-Gibbs theory [29,30], the constitutive relationship between the relaxation of mobile amorphous component and the degree of crystallinity is formulated as a function of glass transition temperature (T_g) of semi-crystalline SMPs. The modified Avrami theory [31] is then introduced to describe the melting transition and thermodynamics of crystalline component. Furthermore, rigid amorphous component is then introduced into the interfaces between mobile amorphous and crystalline components, and effect of three components on the thermomechanical behavior are formulated using the multi-modal commutative and cooperative models to characterize the thermodynamics and shape recovery behavior of the semi-crystalline SMPs [32,33]. Finally, all the obtained analytical results are compared with the experimental ones reported in Ref. [17,34] in order to verify the newly proposed model.

2. Thermodynamic model of semi-crystalline SMPs

2.1 Extended three-phase model

Thermomechanical behavior of semi-crystalline SMPs is strongly dependent on their morphologies [35]. A explained in introduction, based on the three-phase model [22], the semi-crystalline SMPs are composed of three parts, i.e. crystalline component, the mobile amorphous component and rigid amorphous component, the last of which is located at the interfacial regions between the crystalline and mobile amorphous ones, as shown in Figure 1. To characterize these unique three-phase

features in semi-crystalline SMPs, Takayanagi principle is employed and thus the storage modulus ($E(T)$) has the following form [32],

$$E(T) = 1/\left(\frac{\lambda}{\varphi E_c(T) + (1-\varphi) E_r(T)} + \frac{1-\lambda}{E_m(T)} \right) \tag{1}$$

where E_c , E_r and E_m are the storage moduli of the crystalline, rigid amorphous and mobile amorphous components, respectively, λ and φ are the dimensionless width and length of the crystalline component along the loading direction, respectively.

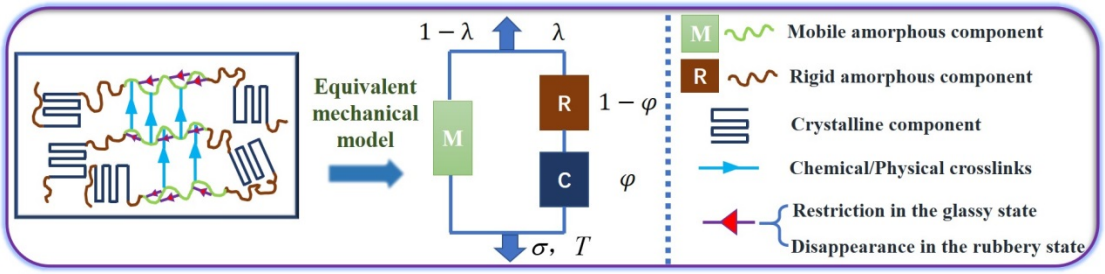

Figure 1. Illustration of three-phase feature in a semi-crystalline SMP composed of mobile amorphous, rigid amorphous and crystalline components, based on the three-phase model [22].

In Equation (1), the parameters λ and φ can be used to characterize the volume fraction of three components in the semi-crystalline polymers, and they can be determined using a temperature modulated differential scanning calorimetry (TMDSC) method [36]. The volume fractions of these three components can be written as,

$$W_m = \frac{\Delta C_p}{\Delta C_{p0}} = 1\text{-}\lambda \; ; \; W_c = \frac{\Delta h}{\Delta h_0} = \lambda\varphi \; ; \; W_r = 1 - W_m - W_c = \lambda(1-\varphi) \tag{2}$$

where W_m , W_r and W_c are the volume fractions of the mobile amorphous, rigid amorphous and crystalline components, respectively. ΔC_p and ΔC_{p0} are the heat

capacities of the semi-crystalline and pure amorphous polymers, respectively. Δh and Δh_0 are the heights of melting peaks of the semi-crystalline and pure amorphous polymers, respectively, from the results of TMDSC [37].

According to the equations (1) and (2), the thermomechanical behavior of semi-crystalline SMPs is critically determined by the parameters of λ and φ, whereas the thermomechanical glass and melting transitions significantly influence these two parameters, according to the Takayanagi principle [32]. Therefore, effects of glass and melting transitions on the thermomechanical behavior of semi-crystalline SMPs will be investigated in the following section.

2.2 Glass transition of the mobile amorphous component

In the semi-crystalline SMPs, the mobile amorphous component enables the polymer with shape memory effect (SME), based on its glass transition. Phase transition theory has therefore been formulated to study the effect of glass transition on the SME of amorphous component [38]. The phase evolution function (ϕ_m) has the following relationship with temperature (T) and time (t) [38],

$$\phi_m(T) = \frac{\varepsilon_{s,m}}{\varepsilon_{pre,m}} = \left(1 - \exp\left(-\frac{\Delta H(T)}{k_b T}\right)\right)^{\frac{t}{\tau_0}} \quad (t = (T - T_i)/q) \tag{3}$$

where $\varepsilon_{s,m}$ is the stored strain, $\varepsilon_{pre,m}$ the pre-deformed strain, $\Delta H(T)$ is the activation energy, k_b is the Boltzmann's constant, τ_0 is the internal relaxation time, T_i is the initial temperature and q is the heating rate.

On the other hand, the confinement effect of crystalline component on the glass transition of mobile amorphous component should be considered in the semi-crystalline SMPs, and their glass transition behavior is different from that of the pure

amorphous SMPs. According to the Adam-Gibbs theory [30], the cooperative rearranging region (CRR) can be employed to describe the cooperative phase transition of mobile amorphous and crystalline components. The domain size ($z(T)$), which indicates the number of the components in a CRR, can be expressed as [39],

$$z(T) = \frac{\ln 2 N k_b T_g}{\Delta C_p (T - T_0)} \tag{4}$$

where N is the overall number of components, T_g is the glass transition temperature of mobile amorphous component, and T_0 is the low-temperature limit where the configuration energy becomes infinitesimal.

Substituting equation (2) into (4), the expression of domain size ($z(T)$) as functions of temperature and volume fraction for the mobile amorphous component is obtained,

$$z(T) = \frac{\ln 2 N k_b T_g}{W_m \Delta C_{p0} (T - T_0)} \tag{5}$$

The relaxation time ($\tau(T)$) of the mobile amorphous component can then be derived from the Adam-Gibbs theory [30],

$$\tau(T) = \tau^* \exp\left(\frac{\Delta\mu}{R}\left(\frac{z(T)}{T} - \frac{1}{T^*}\right)\right) = \tau^* \exp\left(\frac{\Delta\mu}{R}\left(\frac{\ln 2 N k_b T_g}{W_m \Delta C_{p0} T (T - T_0)} - \frac{1}{T^*}\right)\right) \tag{6}$$

where $\Delta\mu$ is the activation energy of per mole mobile amorphous component activated independently, R=8.314J/(mol·K) is the gas constant and τ^* is the relaxation time at temperature T^*.

Table 1. Values of parameters used in equation (6) for relaxation time of semi-crystalline PETs.

W_m(%)	T_g(K)	N	$\Delta C_{p0}(J/(g\cdot K))$	τ^*(min)	T^*(K)

39.1	365	7.2×10^{23}	0.33	1.0×10^{-5}	750
57.5	360	1.2×10^{24}			
100	338	9.3×10^{23}			

Based on the proposed model of equation (6), we have calculated the relaxation time as a function of temperature for the semi-crystalline poly(ethylene terephthalate) (PET), and then compare with the experimental data reported in Ref. [40]. The obtained analytical results are shown in Figure (2). The volume fractions of mobile amorphous components in the PETs using in equation (6) during calculation are 39.1%, 57.5% and 100%, respectively. The values of all the parameters are listed in Table 1. At the 330 K, both the analytical and experimental results present that the relaxation time is increased from 141 s, 9710 s to 43744 s, with a decrease in the volume fraction of the mobile amorphous components from 100%, 57.5% to 39.1%. It is found that the relaxation motion is seriously restricted by decreasing the volume fraction of mobile amorphous component, whereas the volume fraction of crystalline component is therefore increased in the PET. As discussed above, there are cooperative relaxation motions between the mobile amorphous and crystalline components, resulted from their CRRs and cooperative phase transitions based on the Adam-Gibbs theory [30]. Therefore, the relaxation time of the semi-crystalline PET is then increased with the volume fraction of crystalline component.

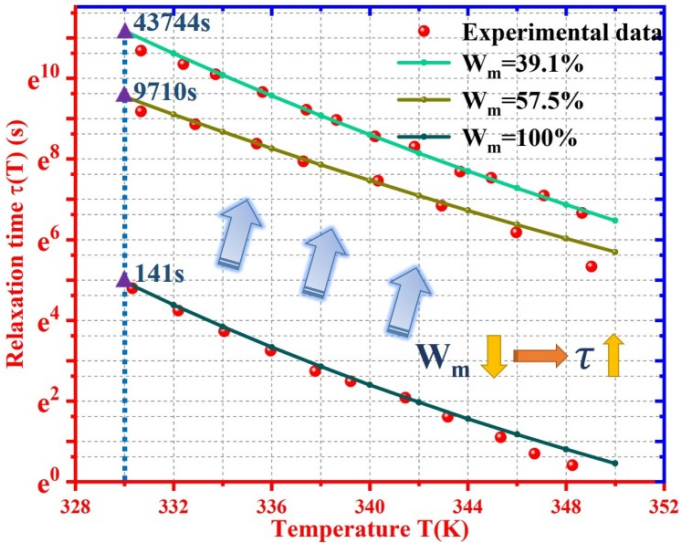

Figure 2. Comparisons between analytical results using the equation (6) and experimental data of relaxation time as a function of temperature for semi-crystalline PETs, reported in Ref. [40].

To further model the phase transition, it is necessary to develop a framework between the activation energy ($\Delta H(T)$) and volume fraction of the mobile amorphous component. According to the Adam-Gibbs theory [30] and equation (5), the activation energy ($\Delta H(T)$) can be rewritten as,

$$\Delta H(T) = z\Delta\mu = \frac{\ln 2 N k_b T_g \Delta\mu}{W_m \Delta C_{p0}(T - T_0)} \tag{7}$$

Combining equations (3) and (7), the phase evolution function (ϕ_m) of the mobile amorphous component has the following constitutive relationship with temperature and volume fraction,

$$\phi_m(T,t) = \frac{\varepsilon_{s,m}}{\varepsilon_{pre,m}} = \left(1 - \exp\left(-\frac{\ln 2 N T_g \Delta\mu}{W_m \Delta C_{p0} T (T - T_0)}\right)\right)^{\frac{t}{\tau_0}} \tag{8}$$

Based on equation (8), we can investigate the effects of volume fraction of mobile amorphous component (W_m) on the phase evolution function (ϕ_m) as a function of

temperature. As shown in Figure 3(a), the phase evolution function (ϕ_m) is gradually decreased with an increase in temperature. Results show that the semi-crystalline SMPs can complete the phase transition (where ϕ_m=0) at 368 K, 372 K, 377 K, 382 K and 385 K, with a decrease in volume fraction from 95%, 90%, 85%, 80% to 75%. Whereas the heating rate (q=2 K/min) and internal time (τ_0=2 min) are kept constants in the analysis. These analytical results reveal that a higher temperature is necessary to help the semi-crystalline SMP to complete the phase transition according to the equation (2), where the volume fraction ($W_m = 1-\lambda$) mobile amorphous component is decreased and the volume fraction ($W_c = \lambda\varphi$) mobile amorphous component is increased.

On the other hand, the simulation results of temperature-dependent phase transition of the semi-crystalline SMPs are also plotted in Figure 3(b). It is found that the heating rate (q) plays a critical role to influence the phase transition, e.g., the phase evolution function is increased to a larger value at the same temperature when the heating rate is increased. The SMPs complete their phase transitions at 382 K, 395 K, 407 K, 410 K and 428 K, when the heating rates are set as 2 K/min, 5 K/min, 15 K/min and 20K/min. The results show that the phase transition of semi-crystalline SMPs is prolonged with an increase in the heating rate, at the same volume fraction of mobile amorphous component W_m=80%.

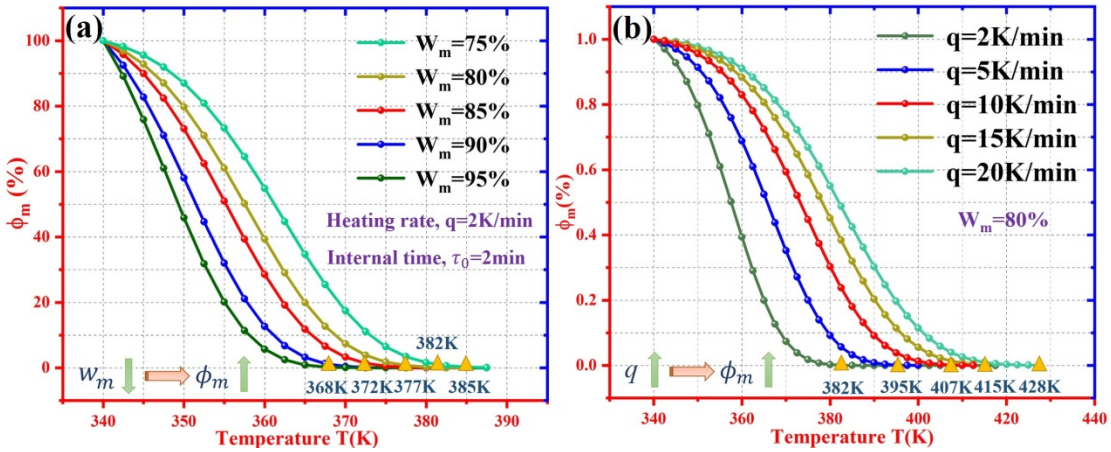

Figure 3. (a) Phase evolution function (ϕ_m) as a function of temperature at various volume fractions of mobile amorphous component of W_m=75%, 80%, 85%, 90% and 95%; (b) Phase evolution function (ϕ_m) as a function of temperature at various heating rates of q=2 K/min, 5 K/min, 10 K/min, 15 K/min and 20K/min.

2.3 Melting transition of crystalline component

For the melting transition of crystalline component, the Avrami theory [31] is used to characterize the dynamic transition behavior of the semi-crystalline SMPs at their melting transition temperatures (T_m). Here the phase evolution function (ϕ_c) of the crystalline component is determined by the stored strain ($\varepsilon_{s,c}$) and the pre-deformed strain ($\varepsilon_{pre,c}$) of the crystalline component in semi-crystalline SMPs, which can be written using the following equation [31],

$$\phi_c(T,t) = \frac{\varepsilon_{s,c}}{\varepsilon_{pre,c}} = \exp\left(-\int_0^t K(T(t))dt\right) \tag{9}$$

where $K(T(t))$ is the kinetic parameter of the melting transition. Based on the Jeziorny method [41], this kinetic parameter is determined by the temperature ($T(t)$),

$$K(T) = K_{\max}\exp(-4\ln 2(T-T_m)^2/D^2) \tag{10}$$

where $K_{\max}$ is the maximum value of kinetic parameter and D is a constant [41].

Substituting equation (10) into (9), the phase evolution function of the crystalline component can be rewritten as,

$$\phi_c(T,t) = \frac{\varepsilon_{s,c}}{\varepsilon_{pre,c}} = \exp\left(-K_{\max}\int_0^t \exp(-4\ln 2(T-T_m)^2/D^2)dt\right) \tag{11}$$

The stored strain (ε_s) of semi-crystalline SMPs is incorporated of those of the mobile amorphous ($\varepsilon_{s,m}$) and crystalline ($\varepsilon_{s,c}$) components. Therefore, the stored strain (ε_s) of semi-crystalline SMP can be obtained based on the equations (8) and (11),

$$\varepsilon_s(T,t) = \varepsilon_{s,m} + \varepsilon_{s,c} = \phi_m(T,t)\varepsilon_{pre,m} + \phi_c(T,t)\varepsilon_{pre,c} \tag{12}$$

Using equation (12), we have calculated the stored strains ($\varepsilon_s(T,t)$) of semi-crystalline epoxy/PCL SMPs with triple-SME, and then compared with those experimental data reported in Ref. [34]. The results are plotted in Figure 4. The T_g of epoxy component is 303 K and the T_m of PCL crystalline component is 337 K. As shown in Figure 4(a), the epoxy acts as the mobile amorphous and rigid amorphous components. While the PCL acts as the crystalline component. Since the T_g of epoxy component is lower than the T_m of PCL crystalline component, the glass transition is firstly achieved at a temperature of 303 K. Then the melting transition is achieved at a temperature of 337 K. Therefore, there is a triple-SME (or a two-step recovery) generated in the epoxy/PCL SMPs [42].

Figure 4(b) plots the numerical results of the stored strains as a function of temperature for the semi-crystalline epoxy/PCL SMP. The experimental data reported

in Ref. [34] and the numerical results obtained using a previously reported model [26] were also collected and plotted for comparisons. The values of parameters used in calculation using the equation (12) are listed in Table 2. It is found that the numerical results obtained from the proposed model fit well with the experimental results. The semi-crystalline epoxy/PCL SMP undergoes the glass transition and the first shape recovery of mobile amorphous epoxy component occurs in the temperature range from 285 *K* to 318 *K*. Then the melting transition and the second shape recovery of crystalline PCL component are achieved in the temperature range from 329 *K* to 345 *K*. There is a plateau region located at the temperature range from 318 *K* to 329 *K* between the first and second shape recoveries.

Table 2. Values of parameters in equation (12) for semi-crystalline epoxy/PCL SMP.

Mobile amorphous component (epoxy)				Crystalline component (PCL)		
$T_g(K)$	$T_0(K)$	τ_0(min)	$\Delta\mu N/\Delta C_{p0}$	$K_{\max}$	$T_m(K)$	D
303.5	288.3	0.58	2335	1.23	337.4	37.8

It should be noted that the first glass transition of epoxy component is resulted from the cooperative relaxation motions of both mobile amorphous and crystalline components, according to the Adam-Gibbs theory [30]. Their CRRs are characterized by the rigid amorphous component in the proposed model, of which the numerical results are more accurate to predict the experimental data in comparison with that of the previous model. Furthermore, the effect of volume fraction (W_m) of mobile amorphous epoxy component on the shape recovery behavior of semi-crystalline epoxy/PCL SMP has been investigated using Equation (12), and the results are shown in Figure 4(c). Based on these numerical results, the SMP completes the glass transition at temperatures of 338.6 K, 329 K, 326 K, 322 K and 314 K, respectively,

when the volume fractions of mobile amorphous epoxy component are increased from 0%, 10%, 15%, 20% to 25%. These analytical results reveal that the two-step shape recovery is also determined by the volume fractions of amorphous and crystalline components [43]. Furthermore, the triple-SME and shape recovery behavior can be designed and tailored by varying volume fractions of amorphous and crystalline components in the semi-crystalline epoxy/PCL SMP.

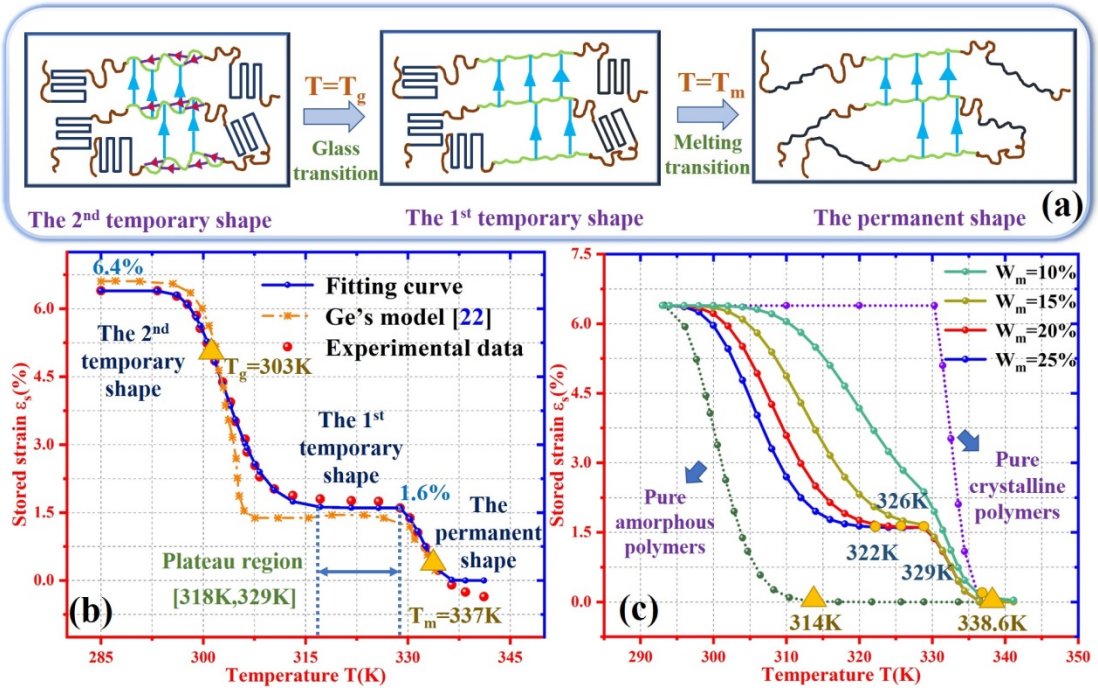

Figure 4. (a) Illustrations of triple-SME in a semi-crystalline SMP, which is incorporated from mobile amorphous, rigid amorphous and crystalline components. (b) Comparisons among simulation results using equation (12), using a previous model [26], and experimental data [34] of the stored strain as a function of temperature for semi-crystalline epoxy/PCL SMP. (c) Simulation results of the stored strain as a function of temperature at various volume fraction of mobile amorphous component of W_m=0%, 10%, 15%, 20%, 25% to 100%.

2.4 Thermodynamics and experimental verification

As discussed in Ref. [44], the storage modulus of the mobile amorphous component (E_m) as a function of temperature can be written as,

$$E_m(T) = E_{m,f}\left(1+\frac{(1-\phi_m(T))(E_{m,a}/E_{m,f}-1)}{1+\alpha\phi_m(T)(E_{m,a}/E_{m,f}-1)}\right) \tag{13}$$

where $E_{m,f}$ and $E_{m,a}$ are the storage moduli of the frozen and active phases in the mobile amorphous component, respectively [44], and α is a fitting constant.

Based on the previous study of the semi-crystalline SMPs [26], the crystalline components cannot resist the external force after their melting transitions. Therefore, we can further modify the relationship between the storage modulus of the crystalline component (E_c) and temperature (T),

$$E_c(T) = E_{c0}\phi_c(T,t) = E_{c0}\exp\left(-K_{\max}\int_0^t \exp(-4\ln 2(T-T_m)^2/D^2)dt\right) \tag{14}$$

where E_{c0} is the storage moduli of the pure crystalline component, without undergoing any melting transition.

In the semi-crystalline SMPs, the rigid amorphous component works at the interfaces between mobile amorphous and crystalline components, thus enabling their cooperative relaxation motions. Once the crystalline component undergoes the melting transition at T_m, the rigid amorphous component is released from the crystalline component and thus will have the same relaxation motion as that of the mobile amorphous component. Therefore, the storage modulus of the rigid amorphous component ($E_r(T)$) can be written using the following relationship,

$$E_r(T) = E_{r0}\phi_c(T,t) + E_{m,a}(1-\phi_c(T,t)) \tag{15}$$

where E_{r0} is the initial storage moduli of the rigid amorphous component.

By substituting equations (13), (14) and (15) into equation (1), the storage modulus of semi-crystalline SMPs can be finally obtained as,

$$\frac{1}{E(T)} = \frac{\lambda}{\varphi E_{c0}\phi_c(T,t) + \varphi E_{r0}\phi_c(T,t) + (1-\varphi)E_r(T)} + \frac{1-\lambda}{E_m(T)} \quad (16)$$

To verify the proposed model on the thermodynamic behavior of semi-crystalline SMPs, we have calculated the moduli results of the semi-crystalline epoxy/PCL and amorphous epoxy SMPs using equation (16), and the obtained results are compared with the experimental data reported in Ref. [34]. The values of parameters used in equation (16) are presented in Table 3. As shown in Figure 5, the storage modulus of amorphous epoxy SMP is gradually decreased from 1345MPa to 6.1 MPa with an increase in temperature from 295 K to 320 K, mainly due to the differences in the glass transitions. On the other hand, the storage modulus of semi-crystalline epoxy/ PCL SMP is decreased from 1345 MPa to 19 MPa owing to the differences in the glass transitions of amorphous epoxy component. Results also show that the storage modulus is further decreased from 19 MPa to 4 MPa in the temperature range from 335 K to 360 K, mainly due to the differences in the melting transitions of crystalline PCL component. The triple-SME and two-step recovery are all characterized and predicted using our newly proposed model, and the fitting curves are in good agreements with the experimental data of semi-crystalline epoxy/PCL SMP [34], as shown in Figure 5.

Table 3**.** Values of parameters in equation (16) for semi-crystalline epoxy/PCL SMP.

$E_{m,f}(MPa)$	$E_{m,a}(MPa)$	$E_{r0}(MPa)$	$E_{c0}(MPa)$	α	λ	φ
1459.3	6.1	1287.7	1407.4	0.47	0.68	0.36

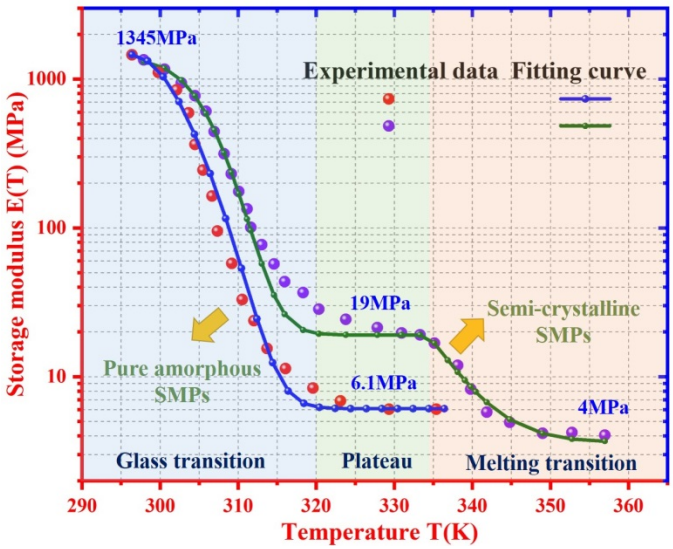

Figure 5. Comparisons between numerical results of equation (16) and the experimental data reported in Ref. [34] of amorphous epoxy and semi-crystalline epoxy/PCL SMPs.

Furthermore, effects of the component composition on the thermodynamic behavior are further investigated for the semi-crystalline SMPs using our proposed model. As shown in Figure 6(a), the plateau modulus is gradually increased from 19 MPa, 30 MPa to 55 MPa with a decrease in the volume fraction of mobile amorphous component (W_m) from 30%, 20% to 10% at T =320 K, with a fixed value of φ=0.423. The working mechanism for the changes of plateau modulus is originated from the increase in volume fractions of rigid amorphous and crystalline components, which play as the CRRs for mobile amorphous component based on the Adam-Gibbs theory [30]. Therefore, the increases in volume fractions of both rigid amorphous and crystalline components are beneficial for the semi-crystalline SMP to achieve a high storage modulus [45].

On the other hand, the effect of volume fraction of crystalline component on the storage modulus as a function of temperature has been investigated, and the obtained results are shown in Figure 6(b). The numerical results reveal that the storage modulus is gradually decreased from 3.1 MPa, 2.1 MPa to 1.2 MPa with an increase in the volume fraction of crystalline component (W_c) from 54%, 63% to 72% at T =355 K, with a fixed value λ =0.9. With an increase in the volume fraction of crystalline component, the volume fraction of rigid amorphous component is therefore decreased, resulting in the decrease of storage modulus.

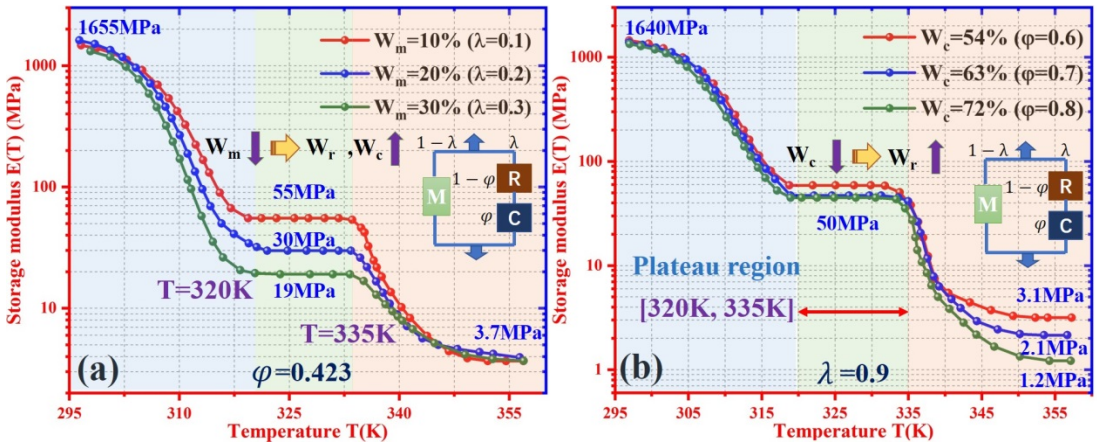

Figure 6. (a) Simulation results of the storage moduli of semi-crystalline SMP with various volume fraction of the mobile amorphous component of W_m=10%, 20% and 30%, whereas φ=0.423 ; (b) Simulation results of the storage moduli of semi-crystalline SMP with various volume fraction of the crystalline component of W_c =54%, 63% and 72%, whereas λ=0.9.

These numerical analyses are helpful to identify the real working mechanism of thermodynamics in the semi-crystalline SMPs. The rigid amorphous component, which plays as the CRR for the cooperative motion of mobile amorphous and crystalline components, determines the thermodynamic behavior of the semi-

crystalline SMP. The SMP will achieve a higher storage modulus when the volume fraction of rigid amorphous component is increased. Therefore, the working mechanism of thermodynamics in the semi-crystalline SMP is originated from the cooperative motions between mobile amorphous and crystalline components.

3. Multiple melting transitions in semi-crystalline SMPs

For the semi-crystalline SMPs, the multiple melting transitions could provide many temporary shapes and enable them with multi-SMEs. Based on the Boltzmann's superposition principle [46], equation (12) can be further extended as,

$$\varepsilon_s(T,t) = \sum_{i=1}^{n} \varepsilon_{s,m}(i) + \sum_{k=1}^{m} \varepsilon_{s,c}(k) = \sum_{i=1}^{n} \phi_m(i)\varepsilon_{pre,m}(i) + \sum_{k=1}^{m} \phi_c(k)\varepsilon_{pre,c}(k) \tag{17}$$

where n and m are the numbers of glass and melting transitions in the semi-crystalline SMPs, respectively. Parameters i and k indicate the ith glass transition component and the kth melting transition component, respectively.

Equation (17) is used to calculate the stored strains of the PLLA/PDLA/PU triblock with quadruple-SME, and the obtained numerical results are plotted and compared with the experimental data reported in Ref. [17], as shown in Figure 7. Values of parameters used in equation (17) in the calculation are listed in Table 3. Experimental results [17] revealed that the glass and melting transitions of PLLA and PDLA segments were able to store the temporary shapes for the semi-crystalline PLLA/ PDLA/PU SMPs. Based on Figure 7, the first shape recovery of SMPs is induced by the glass transition of PLLA component in the temperature range from 293 K to 333 K. The second shape recovery of SMPs is triggered due to the melting transition of PLLA component in the temperature range from 333 K to 363 K. The third shape recovery is resulted from the melting transition of PDLA component in the

temperature range from 363 K to 403 K. Therefore, a quadruple-SME has been achieved for the semi-crystalline PLLA/PDLA/PU SMP, whereas it takes 16 min, 32.5 min and 19.5 min to complete the three-step recovery process.

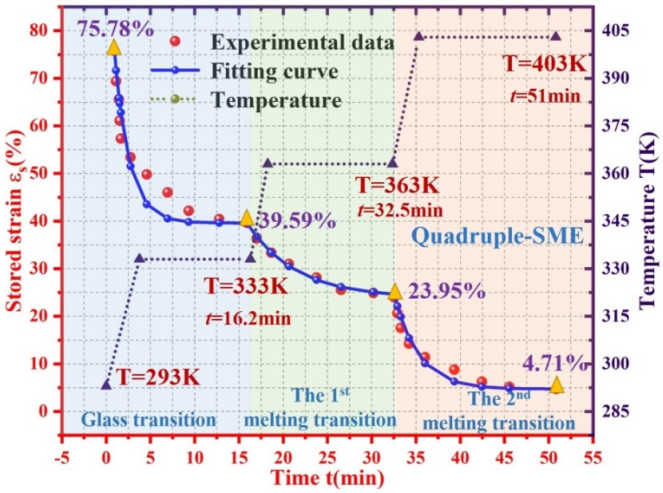

Figure 7. Comparisons of stored strains with respect to recovery time between analytical results and experimental data [17] of semi-crystalline PLLA/PDLA/PU SMP with quadruple-SME.

Table 4. Values of parameters in equations (17) and (18).

Parameter	λ	α	$E_{m,f}$ (MPa)	$E_{m,a}$ (MPa)	T_0 (K)	τ_0 (min)	$T_g(K)$	$N\Delta\mu/W_m\Delta C_{p0}$
Glass transition of PLLA	0.1	0.99	3158.6	7.1	218	5.75	223	598.07
Glass transition of PDLA	0.4	1.01	2557.6	5.6	255.8	4.58	253	153.62

Parameter	λ	φ	E_{c0} (MPa)	E_{r0} (MPa)	T_m (K)	D	K_{max}	$\sigma_i(0)$ (MPa)	T^* (K)	μ_c (MPa)
Melting transition of PLLA	0.2	0.58	3002.3	2425.7	360	798	0.03	1.6	620	2.1
Melting transition of PDLA	0.3	0.73	3233.4	2677.8	400	382	0.05	3.2	710	2.4

Furthermore, the semi-crystalline PLLA/PDLA/PU SMP can reveal two glass

transitions and two melting transitions, thus enabling a quadruple-SME. The Takayanagi principle [32] is employed to characterize the morphology feature of semi-crystalline PLLA/PDLA/PU SMP, as illustrated in Figure 8(a). The symbols of M1, R1 and C1 represent the mobile amorphous component, rigid amorphous component and crystalline component of PLLA segment, respectively. While symbols of M2, R2 and C2 represent the mobile amorphous component, rigid amorphous component and crystalline component of PDLA segment, respectively. According to the Takayanagi principle [32], the storage modulus of semi-crystalline PLLA/PDLA/PU SMP can be obtained by expansion of equation (16), e.g.,

$$\frac{1}{E(T)} = \sum_{i=1}^{n} \frac{\lambda_m(i)}{E_m(i)} + \sum_{k=1}^{m} \frac{\lambda_c(k)}{\phi_c(k)E_c(k) + \phi_c(k)E_r(k) + (1-\phi_c(k))E_r(k)} \tag{18}$$

The numerical results of storage moduli obtained using the proposed model of equation (18) for the semi-crystalline PLLA/PDLA/PU SMP have been plotted in Figure 8(b), which has also included the experimental data obtained from the Ref. [17] for comparisons. Values of parameters used in equation (18) are listed in Table 3. It is found that the analytical results from the proposed model are in good agreement with the experimental ones. The storage modulus is sequentially decreased from 2149 MPa to 78 MPa due to the glass transitions of PLLA segment; from 78 MPa to 20 MPa due to the glass transition of PDLA segment; from 20 MPa to 5.3 MPa due to the melting transition of PLLA segment; and from 5.3 MPa to 0.33 MPa due to the melting transition of PDLA segment. Clearly, the SMP presents a quadruple-SME and achieves a four-step recovery behavior with an increase in temperature.

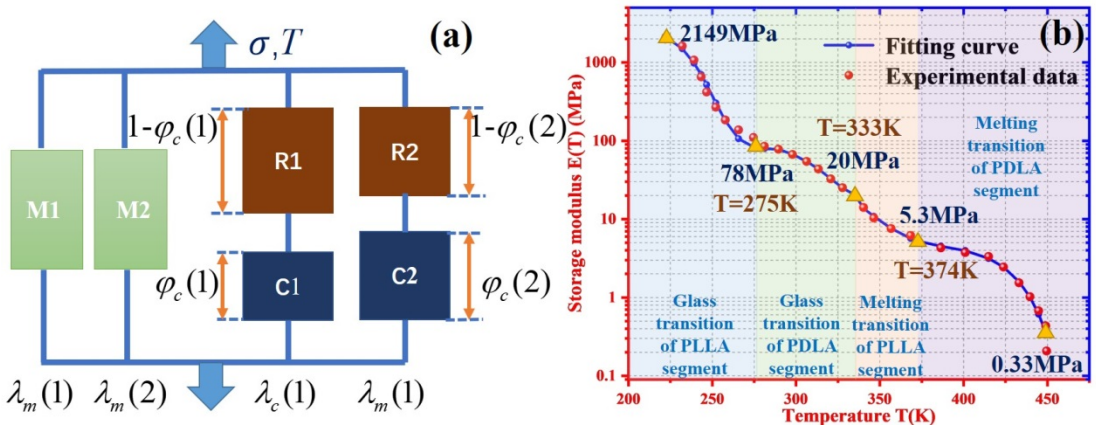

Figure 8. (a) Illustration of the morphology feature of semi-crystalline PLLA/PDLA/PU SMP undergoing two glass and two melting transitions, based on the Takayanagi principle [32]; (b) Comparison between calculation results of equation (18) and experimental data [17] of the storage modulus as a function of temperature in semi-crystalline PLLA/PDLA/PU SMP.

4. Modelling of temperature memory effect (TME) in semi-crystalline SMPs

According to the previous studies [47,48], the programming thermomechanical history has a significantly effect on the shape memory behavior of SMPs. The TME has been identified as the capability of amorphous SMP to memorize the deformation temperature (T_d), which plays an essential role to determine the recovery temperature. Therefore, study on the TME is helpful to explore the thermodynamics in SMP.

Based on the phase transition theory [38], the mobile amorphous component is composed of both the active and frozen phases. During the glass transition, there is a phase transition from the frozen phase into the active one with an increase in temperature. Generally, this constitutive stress-strain relationship is governed by the Maxwell model with a multi-branch model [49],

$$\sigma_m(T,t)=(1-\phi_m(T,t))E_{m,a}\varepsilon_m(t)+\phi_m(T,t)E_{m,f}\int_0^t \frac{d\varepsilon_m(s)}{dt}\exp\left(-\frac{t-s}{\tau(T)}\right)ds \quad (19)$$

where σ_m is the stress and $\varepsilon_m(s)$ is the strain at the time s.

On the other hand, it is necessary to establish the constitutive stress-strain relationships for the rigid amorphous and crystalline components, which work as another branch in the multi-branch model. In the previous work [50], experimental results reveal that there are too many voids between the amorphous and crystalline components under large deformations of the semi-crystalline polyamide 6. In this study, we consider a finite deformation of the semi-crystalline SMPs, thus there will be no voids generated owing to the rigid amorphous component. This will be induced by the strong bonding between mobile amorphous and crystalline components [51,52]. Here the stress of the rigid amorphous component can be written as [51,52],

$$\sigma_r(T,t) = \sigma_y(T,\dot{\varepsilon}_r)\phi_c(T,t)(1-\exp(-A\dot{\varepsilon}_r t)) \tag{20}$$

where $\dot{\varepsilon}_r$ and σ_y are the strain rate and yielding stress of the rigid amorphous component, respectively.

According to the compensation law [53], the yielding stress ($\sigma_y(T,\dot{\varepsilon}_r)$) of semi-crystalline polymer as a function of strain rate ($\dot{\varepsilon}_r$) can be expressed as,

$$\frac{\sigma_y(T,\dot{\varepsilon}_r)}{T} = \frac{\sigma_i(0)-\left(\sigma_i(0)T/T^*\right)}{T} + \frac{2.3k_b}{V}\log\left(\dot{\varepsilon}_r/\dot{\varepsilon}_{r0}\right) \tag{21}$$

where $\sigma_i(0)$ is the internal stress at T =0 K and $\dot{\varepsilon}_{r0}$ is the referenced strain rate.

At a finite strain, it is assumed that the stress on crystalline component follows neo-Hookean principle, thus can be obtained by Cauchy stress (σ_c) function [26],

$$\sigma_c = \sigma_r(T,t) = \mu_c\phi_c(T)\left((\varepsilon_c+1)^2 - 1/(\varepsilon_c+1)\right) \tag{22}$$

where μ_c is the shear modulus of the crystalline component. Since the rigid amorphous component is in a series connection with the crystalline component, then we can assume $\sigma_c = \sigma_r(T,t)$.

According to the Takayanagi principle [32], the formulate of the stress (σ) and strain (ε) for the semi-crystalline SMPs can be obtained,

$$\sigma(T,t)=1/\left(\sum_{i=1}^{n}\frac{\lambda_m(i)}{\sigma_m(i)}+\sum_{k=1}^{m}\frac{\lambda_c(k)}{\sigma_c(k)}\right)=1/\left(\sum_{i=1}^{n}\frac{\lambda_m(i)}{\sigma_m(i)}+\sum_{k=1}^{m}\frac{\lambda_c(k)}{\mu_c(k)\phi_c(k)\left((\varepsilon_c(k)+1)^2\text{-}1/(\varepsilon_c(k)+1)\right)}\right) \quad (23a)$$

$$\varepsilon(T,t)=\varepsilon_m(i)=(1-\varphi_c(k))\varepsilon_r(k)+\varphi_c(k)\varepsilon_c(k) \quad (23b)$$

The effects of deformation temperature and mechanical loading stress on the TME have been investigated for the semi-crystalline PLLA/PDLA/PU SMPs, and the results are shown in Figures 9(a), 9(b) and 9(c). In this case, the deformation temperatures are T_d=363 K, 373 K and 383 K, and the mechanical loading stresses are σ =1.15MPa, 1.3 MPa, and 1.4 MPa. Values of parameters used in equations 23(a) and 23(b) in the calculation are listed in Table 4. The experimental data reported in Ref. [17] for the semi-crystalline PLLA/PDLA/PU SMPs have been employed for comparison and verification. These numerical results fit well with the experimental ones, and the degree of deviation between the numerical and experimental ones [17] are 9.92%, 8.3% and 5.2% at various deformation temperatures of T_d=363 K, 373 K and 383 K, respectively, as shown in Figure 9(d). The numerical and experimental results reveal that the stored mechanical energy, which is influenced by both the deformation temperature and mechanical loading stress, plays an essential role to determine the TME in the semi-crystalline PLLA/PDLA/PU SMP. Therefore, we can conclude that the mechanical loading stress has a direct effect on the stored

mechanical energy. While the deformation temperature has also a significant effect on the stored mechanical energy, of which the SME has the same working mechanism as that of the TME in the other types of SMPs [42,47,48].

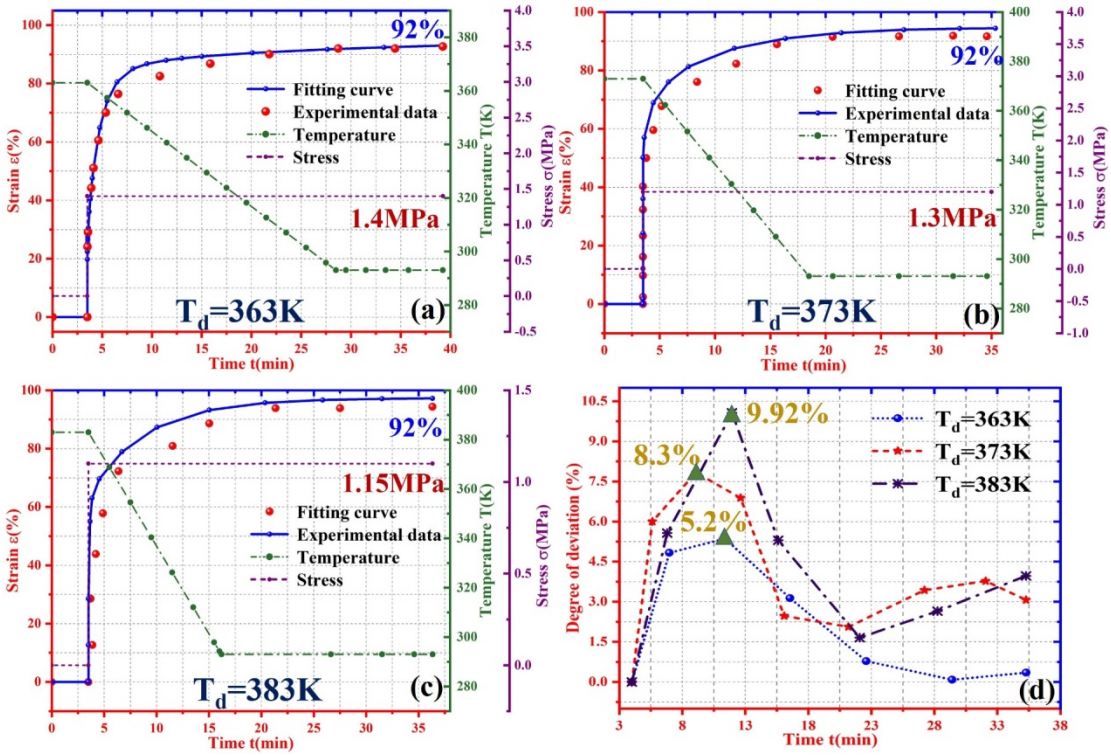

Figure 9. Comparison between analytical results obtained using the equation (23) and the experimental data [17] for the strain as a function of relaxation time. (a) At T_d =363 K and σ =1.4 MPa. (b) At T_d =373 K and σ =1.3 MPa; (c) At T_d =383 K and σ =1.15MPa. (d) The degree of deviation between numerical and experimental results at the temperature of T_d =363K, 373K and 383K.

5. Conclusions

In this study, a thermodynamic model based on three-phase model and Takayanagi principle was developed to describe the cooperative dynamics and thermomechanical behavior of the semi-crystalline SMPs with the multi-SMEs and TME. The cooperative dynamics and motions of amorphous and crystalline components have

been formulated using the extended Adam-Gibbs theory and three-phase model. The phase transition theory and the modified Avrami theory have then been applied to characterize the glass and melting transitions, respectively. Furthermore, the commutative glass and melting transitions have been introduced into the SMPs, and the triple-SME, quadruple-SME and quintuple-SME have been achieved. The constitutive relationships of these multi-SMEs in the semi-crystalline SMPs have been modelled and verified by the experimental results. Finally, the accuracy of analytical results is examined using experimentally obtained relaxation and thermomechanical behaviors reported in the literature, in order to verify the applicability and effectivity of the proposed model. This study is expected to provide a theoretical approach to explore the working principle and cooperative dynamics of multi-SME in semi-crystalline SMP, which provide guidelines for designing desirable relaxation and thermomechanical behaviors for the SMPs.

Acknowledgements

This work was financially supported by the National Natural Science Foundation of China (NSFC) under Grant No. 11725208 and UK Newton Mobility Grant (IE161019) through Royal Society and NFSC.

References

[1] J. Li, T. Liu, S. Xia, Y. Pan, Z. Zheng, X. Ding, Y. Peng, A versatile approach to achieve quintuple-shape memory effect by semi-interpenetrating polymer networks containing broadened glass transition and crystalline segments, J. Mater. Chem. 21 (2011) 12213–12217.

[2] A. Lendlein, O.E.C. Gould, Reprogrammable recovery and actuation behaviour

of shape-memory polymers, Nat. Rev. Mater. 4 (2019) 116–133.

[3] X. Wang, Y. Liu, H. Lu, Y.Q. Fu, On the free-volume model of multi-shape memory effect in amorphous polymer, Smart Mater. Struct. 28 (2019) 125012.

[4] A.D.M. Charles, A.N. Rider, S.A. Brown, C.H. Wang, Improving the actuation performance of magneto-polymer composites by silane functionalisation of carbonyl-iron particles, Compos. Part B Eng. 196 (2020) 108091.

[5] A.D.M. Charles, A.N. Rider, S.A. Brown, C.H. Wang, Improving the actuation performance of magneto-polymer composites by silane functionalisation of carbonyl-iron particles, Compos. Part B Eng. 196 (2020) 108091.

[6] H. Lu, J. Gou, J. Leng, S. Du, Magnetically aligned carbon nanotube in nanopaper enabled shape-memory nanocomposite for high speed electrical actuation, Appl. Phys. Lett. 98 (2011) 1–4.

[7] M. Baniasadi, A. Foyouzat, M. Baghani, Multiple Shape Memory Effect for Smart Helical Springs with Variable Stiffness over Time and Temperature, Int. J. Mech. Sci. 182 (2020) 105742.

[8] Y.F. Zhang, N. Zhang, H. Hingorani, N. Ding, D. Wang, C. Yuan, B. Zhang, G. Gu, Q. Ge, Fast-Response, Stiffness-Tunable Soft Actuator by Hybrid Multimaterial 3D Printing, Adv. Funct. Mater. 29 (2019) 1–9.

[9] M. Baniasadi, E. Yarali, A. Foyouzat, M. Baghani, Crack self-healing of thermo-responsive shape memory polymers with application to control valves, filtration, and drug delivery capsule, Eur. J. Mech. A/Solids. 85 (2021) 104093.

[10] G.I. Peterson, E.P. Childers, H. Li, A. V. Dobrynin, M.L. Becker, Tunable Shape Memory Polymers from α-Amino Acid-Based Poly(ester urea)s, Macromolecules. 50 (2017) 4300–4308.

[11] R. Xiao, J. Guo, D.L. Safranski, T.D. Nguyen, Solvent-driven temperature memory and multiple shape memory effects, Soft Matter. 11 (2015) 3977–3985.

[12] H. Lu, X. Wang, K. Yu, Y. Fu, J. Leng, A thermodynamic model for tunable multi-shape memory effect and cooperative relaxation in amorphous polymers, Smart Mater. Struct. 28 (2019) 025031.

[13] J. Zhou, Q. Li, S.A. Turner, V.S. Ashby, S.S. Sheiko, Isothermal programming of triple shape memory, Polymer. 72 (2015) 464–470.

[14] J. Li, T. Liu, S. Xia, Y. Pan, Z. Zheng, X. Ding, Y. Peng, A versatile approach to achieve quintuple-shape memory effect by semi-interpenetrating polymer networks containing broadened glass transition and crystalline segments, J. Mater. Chem. 21 (2011) 12213–12217.

[15] U. Nöchel, C.S. Reddy, N.K. Uttamchand, K. Kratz, M. Behl, A. Lendlein, Shape-memory properties of hydrogels having a poly(ε-caprolactone) crosslinker and switching segment in an aqueous environment, Eur. Polym. J. 49 (2013) 2457–2466.

[16] I. Bellin, S. Kelch, R. Langer, A. Lendlein, Polymeric triple-shape materials, Proc. Natl. Acad. Sci. U. S. A. 103 (2006) 18043–18047.

[17] J. Zhou, H. Cao, R. Chang, G. Shan, Y. Bao, P. Pan, Stereocomplexed and Homochiral Polyurethane Elastomers with Tunable Crystallizability and Multishape Memory Effects, ACS Macro Lett. 7 (2018) 233–238.

[18] Y. Li, Z. Liu, A novel constitutive model of shape memory polymers combining phase transition and viscoelasticity, Polymer 143 (2018) 298–308.

[19] X. Wang, H. Lu, Y.Q. Fu, J. Leng, S. Du, Collective and cooperative dynamics in transition domains of amorphous polymers with multi-shape memory effect, J. Phys. D. Appl. Phys. 53 (2020) 095301.

[20] J. Diani, P. Gilormini, C. Frédy, I. Rousseau, Predicting thermal shape memory of crosslinked polymer networks from linear viscoelasticity, Int. J. Solids Struct. 49 (2012) 793–799.

[21] X. Wang, H. Lu, N. Wu, D. Hui, M. Chen, Y.Q. Fu, Cooperative principle in multiple glass transitions and strain relaxations of thermochemically responsive shape memory polymer., Smart Mater. Struct. 28 (2019) 085011.

[22] B. Wunderlich, Effect of decoupling of molecular segments, microscopic stress-transfer and confinement of the nanophases in semicrystalline polymers, Macromol. Rapid Commun. 26 (2005) 1521–1531.

[23] P. Da Hong, W.T. Chuang, W.J. Yeh, T.L. Lin, Effect of rigid amorphous phase on glass transition behavior of poly(trimethylene terephthalate), Polymer. 43 (2002) 6879–6886.

[24] J. Jäckle, Models of the glass transition, Reports Prog. Phys. 49 (1986) 171–231.

[25] F. Hamonic, D. Prevosto, E. Dargent, A. Saiter, Contribution of chain alignment and crystallization in the evolution of cooperativity in drawn polymers, Polymer. 55 (2014) 2882–2889.

[26] Q. Ge, X. Luo, C.B. Iversen, P.T. Mather, M.L. Dunn, H.J. Qi, Mechanisms of triple-shape polymeric composites due to dual thermal transitions, Soft Matter. 9 (2013) 2212–2223.

[27] Q. Ge, X. Luo, C.B. Iversen, H.B. Nejad, P.T. Mather, M.L. Dunn, H. Jerry Qi, A finite deformation thermomechanical constitutive model for triple shape polymeric composites based on dual thermal transitions, Int. J. Solids Struct. 51 (2014) 2777–2790.

[28] S. Moon, I.J. Rao, S.A. Chester, Triple Shape Memory Polymers: Constitutive Modeling and Numerical Simulation, J. Appl. Mech. Trans. ASME. 83 (2016) 1–18.

[29] G. Adam, J.H. Gibbs, On the temperature dependence of cooperative relaxation properties in glass-forming liquids, J. Chem. Phys. 43 (1965) 139–146.

[30] S. Matsuoka, Entropy, free volume, and cooperative relaxation, J. Res. Natl. Inst. Stand. Technol. 102 (1997) 213.

[31] M. Avrami, Kinetics of phase change. I: General theory, J. Chem. Phys. 7 (1939) 1103–1112.

[32] R.A. Dickie, Heterogeneous polymer–polymer composites. I. Theory of viscoelastic properties and equivalent mechanical models, J. Appl. Polym. Sci. 17 (1973) 45–63.

[33] H. Lu, X. Wang, Z. Xing, Y.Q. Fu, A cooperative domain model for multiple phase transitions and complex conformational relaxations in polymer with shape memory effect, J. Phys. D. Appl. Phys. 52 (2019) 245301.

[34] X. Luo, P.T. Mather, Triple-shape polymeric composites (TSPCs), Adv. Funct. Mater. 20 (2010) 2649–2656.

[35] A. Jonas, R. Legras, Relation between PEEK Semicrystalline Morphology and Its Subglass Relaxations and Glass Transition, Macromolecules. 26 (1993) 813–824.

[36] N. Delpouve, A. Saiter, J.F. Mano, E. Dargent, Cooperative rearranging region

size in semi-crystalline poly(l-lactic acid), Polymer. 49 (2008) 3130–3135.

[37] J. Pak, M. Pyda, B. Wunderlich, Rigid amorphous fractions and glass transitions in poly(oxy-2,6-dimethyl-1,4-phenylene), Macromolecules. 36 (2003) 495–499.

[38] Y. Liu, K. Gall, M.L. Dunn, A.R. Greenberg, J. Diani, Thermomechanics of shape memory polymers: Uniaxial experiments and constitutive modeling, Int. J. Plast. 22 (2006) 279–313.

[39] J. Jäckle, Models of the glass transition, Reports Prog. Phys. 49 (1986) 171–231.

[40] N.M. Alves, J.F. Mano, E. Balaguer, J.M. Meseguer Dueñas, J.L. Gómez Ribelles, Glass transition and structural relaxation in semi-crystalline poly(ethylene terephthalate): A DSC study, Polymer. 43 (2002) 4111–4122.

[41] Jeziorny A., 'Parameters characterizing kinetics of nonisothermal crystallization of poly(ethylene-terephthalate) determined by DSC, Polymer. 19 (1978) 1142–1144.

[42] K. Yu, T. Xie, J. Leng, Y. Ding, H.J. Qi, Mechanisms of multi-shape memory effects and associated energy release in shape memory polymers, Soft Matter. 8 (2012) 5687–5695.

[43] J. Li, T. Xie, Significant impact of thermo-mechanical conditions on polymer triple-shape memory effect, Macromolecules. 44 (2011) 175–180.

[44] Q. Yang, G. Li, Temperature and rate dependent thermomechanical modeling of shape memory polymers with physics based phase evolution law, Int. J. Plast. 80 (2016) 168–186.

[45] T. Xie, X. Xiao, Y.T. Cheng, Revealing triple-shape memory effect by polymer bilayers, Macromol. Rapid Commun. 30 (2009) 1823–1827.

[46] H. F. Brinson, Polymer Engineering Science and Viscoelasticity: An Introduction, Springer, New York, 2007.

[47] L. Sun, W.M. Huang. Mechanisms of the multi-shape memory effect and temperature memory effect in shape memory polymers, Soft Matter 6 (2010) 4403–4406.

[48] T. Xie, K. Page, S. Eastman, Strain based temperature memory effect for Nafion and its molecular origins, Adv. Funct. Mater. 21 (2011) 2057–2066.

[49] K.K. Westbrook, P.H. Kao, F. Castro, Y. Ding, H. Jerry Qi, A 3D finite

deformation constitutive model for amorphous shape memory polymers: A multi-branch modeling approach for nonequilibrium relaxation processes, Mech. Mater. 43 (2011) 853–869.

[50] L. Laiarinandrasana, O. Klinkova, F. Nguyen, H. Proudhon, T.F. Morgeneyer, W. Ludwig, Three dimensional quantification of anisotropic void evolution in deformed semi-crystalline polyamide 6, Int. J. Plast. 83 (2016) 19–36.

[51] A. Thévenon, R. Fulchiron, A thermomechanical modeling approach of the structural changes in semi-crystalline polymers under elongational strain, J. Mater. Sci. 49 (2014) 433–440.

[52] F. Zeng, P. Le Grognec, M.F. Lacrampe, P. Krawczak, A constitutive model for semi-crystalline polymers at high temperature and finite plastic strain: Application to PA6 and PE biaxial stretching, Mech. Mater. 42 (2010) 686–697.

[53] O. Gueguen, J. Richeton, S. Ahzi, A. Makradi, Micromechanically based formulation of the cooperative model for the yield behavior of semi-crystalline polymers, Acta Mater. 56 (2008) 1650–1655.